Gasoline selective Fischer-Tropsch synthesis in structured bifunctional catalysts

Chunxiang Zhu, George M. Bollas*

Department of Chemical & Biomolecular Engineering, University of Connecticut, Storrs, 159 Discovery Dr., Storrs, CT 06269, USA

ARTICLE INFO

Keywords:
Fischer-Tropsch synthesis
Gasoline selective
Structured catalyst
ZSM-5
Bifunctional catalyst

ABSTRACT

The need for energy independence and security has refocused research on Fischer-Tropsch Synthesis (FTS) and its capability to selectively produce short and branched hydrocarbons. In this work, FTS selectivity to gasoline-range products was explored as a catalysis and process engineering problem. Novel structured catalysts for in situ upgrading of FTS products to gasoline-range hydrocarbons were successfully synthesized by coating controlled-thickness ZSM-5 films on the surface of $Co-Al_2O_3$/monolith substrates. These catalysts were synthesized on the premise that the monolith serves as an efficient mass and heat transfer structure, while the ZSM-5 layer functions as a hydrocarbon cracking and isomerization agent. Compared to traditional diesel-selective FTS, considerably higher quantity and quality of gasoline-range products were achieved with these bi-layered/bi-functional catalysts. Oil products with gasoline yield higher than 65 wt.% and selectivity to isomers and olefins greater than 70 wt.% were formed at relatively high temperature (230 °C) and intermediate pressure (12 bar), without compromising CO conversion, which remained as high as 79%.

1. Introduction

According to the U.S. Department of Energy [1], the high gasoline demand in the U.S. creates a market for high-octane hydrocarbons from alternative domestic sources. The U.S. transportation infrastructure relies heavily on gasoline as the prime liquid fuel. Given the limited success in converting biomass selectively to biofuels [2,3], the dependency of the US transportation sector on foreign petroleum seems unavoidable [4,5]. The shortage of transportation fuels can be mitigated with gas/coal/biomass to liquids (XTL) processes. This is in part due to the newly discovered vast reserves of domestic natural gas, which provides a versatile resource for fuels production and energy generation. Among the various options for the conversion of gas to liquids, Fischer-Tropsch Synthesis (FTS) is a proven process for the production of linear hydrocarbons in the diesel range, from synthesis gas (produced via the reforming or partial oxidation of natural gas). In that context, it is of interest to explore FTS in terms of its capacity for substantial gasoline production, if modifications are to be made to improve its gasoline selectivity and quality.

The recent need for utilization of stranded natural gas from remote locations producing shale oil or shale gas has refocused research on GTL processes and specifically Fischer-Tropsch Synthesis (FTS), as a prime candidate for process intensification and modular manufacturing. However, Fischer-Tropsch is normally a very large-scale process involving complex heat transfer and separation steps. Review of FTS reactor designs, reveals a past trend to design very complex reactors with focus on providing excellent isothermality. Temperature gradients are the major reason of low FTS selectivity. Therefore, FTS reactors include multi-tubular fixed bed reactors dipped in boiling water; slurry bed column reactors, in which synthesis gas is bubbled through a slurry of heavy liquid products and catalyst particles; and gas-solid fluidized-bed reactors or circulating fluidized bed reactors, which offer excellent capacities but suffer from attrition, temperature gradients and difficulty to separate waxes from solids. In this context, FTS intensification or modularization may sound as an oxymoron. Prior work [6–8] has shown excellent results with intensified rectors, such as microreactors, structured reactors and fixed beds with advanced core-shell catalyst loading. FTS is one gas-to-liquids (GTL) process which can be a solution to the transportation issues associated with stranded natural gas and certainly a major challenge to overcome lies in its scalability and uncertainty in its inputs.

FTS using cobalt catalysts has been studied extensively for diesel production in various reactor configurations [9–11]. Despite its commercial success, many challenges still exist in conventional FTS reactors. Fixed bed FTS reactors exhibit large pressure drops, catalyst deactivation, and inefficient control of the reactor temperature [7,12,13]. Fluidized bed FTS reactors experience challenges in the separation of the products from the catalyst, along with catalyst attrition

and deactivation [7,13,14]. Conventional sphere or pellet catalysts pose diffusion limitations to the FTS process, which can lead to high local H_2 concentrations, favoring unwanted light hydrocarbons, linear olefins, and paraffins of low octane number [15,16]. To address these issues, Guettel et al. [17] conducted experiments with cobalt-based monolithic catalysts. They concluded that due to the slug flow regime of monolithic catalysts, higher reaction rates at comparable methane selectivity are feasible. Moulijn and coworkers [6,18] extensively studied preparation methods for coated monolithic FTS catalysts. By tuning the coating thickness, selective FTS with high olefin to paraffin ratios was shown to be feasible. Monolithic catalysts can be operated at low pressure-drops, high geometric surface-areas, high mass-transfer coefficients, and short diffusion lengths, thus relaxing the mass and heat transfer limitations of spherical and pellet catalysts and decreasing olefin reabsorption [6–8,15,19].

Targeting specific carbon number groups is not feasible with the use of advanced reactor designs alone. The Anderson-Schulz-Flory (ASF) distribution poses an upper bound on the theoretical FTS selectivity to gasoline (C_5-C_{12}) at ~48 wt.% in conventional reactors [20–23]. Tsubaki and co-workers [24–30] tried to overcome this barrier by depositing ZSM-5 as an outer shell on conventional FTS catalysts. Their hypothesis was that the ZSM-5 membrane could force the long-chain FTS products to diffuse out through the zeolitic shell and thus have a high probability of undergoing secondary acid-catalyzed reactions. Different types of catalysts were synthesized in their work, such as: core-shell catalysts prepared by hydrothermal coating of HZSM-5 on Co/Al₂O₃ pellets; capsule catalysts by direct coating of HZSM-5 on Co/SiO₂ pellets; Co/SiO₂ + ZSM-5 as the first reaction step catalyst and Pd/SiO₂ + ZSM-5 as the second step catalyst; and hybrid catalysts comprising ZSM-5 and Pd/SiO₂. These catalysts were observed to be capable of direct synthesis of middle range iso-paraffins from syngas. In order to achieve high CO conversion, a higher temperature of 260 °C was recommended, with a concomitant penalty of high CH_4 and CO_2 selectivity.

In this work, we explore the feasibility of combining the advantages of monolithic catalysts and ZSM-5 membrane coating to formulate a highly active and gasoline selective catalyst. We build on the advantages of micro-reactors in scaling and control, which translates to rapid technology transfer and commercialization. In contrast to conventional catalysts, structured catalysts offer low pressure drop, high geometric surface area, high mass transfer coefficients, and short diffusion lengths. The thickness of the catalyst layer can also be adjusted to achieve catalyst effectiveness factors close to unity [7,8,15]. The hypothesis of this work is that the use of bifunctional catalysts, containing FTS active sites and acid catalysts in a bi-layered arrangement in monolith reactors, can improve gasoline selectivity via oligomerization, aromatization, and isomerization reactions without sacrificing CO conversion. Therefore, we explore the potential of structured bifunctional catalysts as candidates for intensified FTS processes selective to high-quality gasoline production. The effectiveness and selectivity of these catalysts were studied in a range of pressures and temperatures. As shown in the following, highly active structured catalysts, capable of enabling high selectivity to branched hydrocarbons in the C_5-C_{12} range, were synthesized and tested.

2. Description of experimental facilities and methods

2.1. Multi-layer monolith catalyst synthesis

The structured catalysts were synthesized on cordierite monolith substrates (2MgO:2Al₂O₃:5SiO₂, Corning, 200 cpsi, L: 7.5 cm), shaped to fit in the 0.5″ ID reactor. Alumina wash-coating solution was prepared, by adding 5 g Boehmite (Al₂O₃, 20% in H₂O, Alfa Aesar) and 30 g deionized water into 25 g γ-Al₂O₃ (99.97%, 3-micron APS powder, 80-120 m²/g surface area, Sigma Aldrich). The mixture was stirred well to achieve homogeneous slurry. The monoliths, pretreated at 120 °C, were immersed in the wash-coating solution for 1 min, and the excess solution was gently blown off with pressurized air. After wash-coating, the monoliths were dried at 120 °C for 4 h and calcined at 400 °C for 12 h. Wash-coating was repeated to tune the thickness of the Al₂O₃ layer. After wash-coating, the active material was deposited by immersing the monolith into a Co(NO₃)₂·6H₂O solution, prepared by dissolving 33.3 g Co(NO₃)₂·6H₂O (98%, Sigma-Aldrich) in 25.6 ml DI water, for 1 min. The excess solution was blown off gently. The catalyst was then dried at 120 °C for 4 h and calcined at 400 °C for 12 h. The final ZSM-5 coating was applied by dip coating the monolith into a NH₄-ZSM-5 slurry, prepared by mixing 20 g NH₄-ZSM-5 (Zeolyst International, 418 m²/g surface area, Si/Al = 80) with 31 ml DI water. The excess solution was again blown off, and the previously described drying and calcination protocols were repeated. Two wash-coatings of Al₂O₃ and a single Co impregnation produced approximately 5 wt.% Co₃O₄ loading on the monolith. Multi-step wash-coating in dilute solutions and careful inspection of the final zeolites reduced or eliminated the potential of axial gradients in the composition and quality of the structured catalysts. Characterization of these catalysts is discussed in Section 3. In the remaining of this article, the notation for the catalyst represents the coating sequence. For instance, ZSM-5/Co-Al₂O₃/M describes that Al₂O₃, Co and ZSM-5 coated the monolith (M) from interior (bare monolith surface) to exterior (final structured catalyst surface). The bare Co-Al₂O₃/M catalyst was used as a baseline to which the ZSM-5 coated catalysts were compared in terms of performance and selectivity. All catalysts were synthesized and characterized thrice and their average properties are reported in Table 1.

2.2. Experimental apparatus and procedure

Fig. 1. presents the FTS microreactor configuration used in this work. A custom-designed fixed bed reactor consisting of a 0.5″ ID and a 12″ long stainless-steel tube (Swagelok) was used for all FTS experiments. Monoliths weighing a total of 2.90 g with ~5 wt.% Co₃O₄ were loaded in the reactor, held in place with quartz wool at both ends of the reactor. The reactor was heated with a tube furnace. A thermocouple at the top of the reactor was used to monitor the reactor entrance temperature and a thermocouple placed at the middle of the outer reactor wall was used to measure and control the reactor temperature. After loading, the catalyst was reduced in situ at 400 °C and 1 atm for 16 h with 50 ml/min pure H₂ flow. Thereafter, the reactor temperature was decreased to 180 °C and Ar was used to purge the reactor. The reactor was pressurized with Ar to 12 bar, controlled by an Equilibar precision back pressure regulator (500 psig max, Cv: 0.07). After stabilization of the pressure at set-point, a premixed 35 ml/min syngas feed, with H₂ to CO ratio of 2:1, was introduced to the reactor. Simultaneously, the temperature was increased to 230 °C at 2 °C/min ramp rate. Ar at

Table 1
Monolithic Catalysts Preparation Parameters Summary.

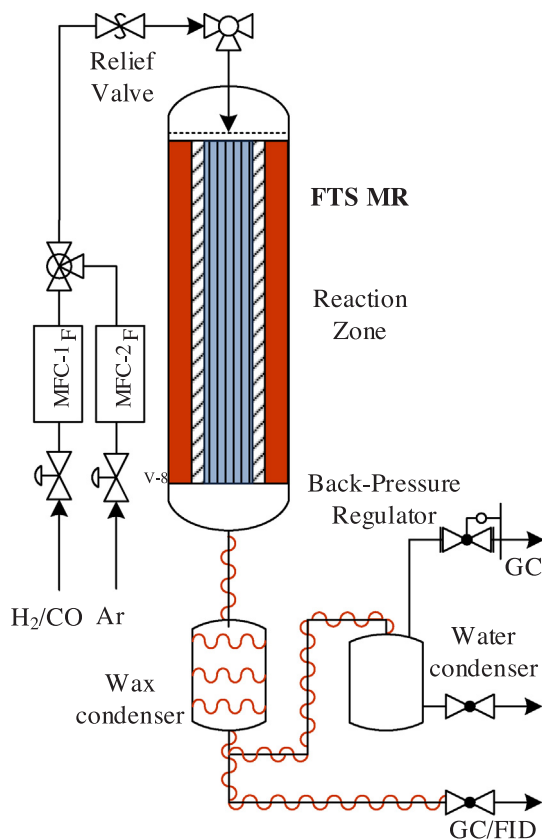| Catalyst	Catalyst loading (g)	Monolith (g)	Al₂O₃ (g)	Co₃O₄ (g)	ZSM-5 (g)
Co-Al₂O₃/M	2.26 ± 0.08	1.42 ± 0.03	0.54 ± 0.06	0.20 ± 0.06	0
ZSM-5/Co-Al₂O₃/M	2.93 ± 0.03	1.42 ± 0.03	0.40 ± 0.08	0.13 ± 0.02	1.03 ± 0.04

Fig. 1. Schematic drawing of the fixed bed reactor used in this work.

10 ml/min was fed continuously to serve as an internal standard. All the gasses were controlled with high-pressure mass flow controllers (BROOKS 5850S). Liquid products were collected in a two-trap system. The wax trap was maintained at 120 °C with temperature-controlled heat tape, while the water condenser was set to room temperature. Gases were analyzed online with gas chromatography (Agilent Micro GC 4900 equipped with PPQ column - 10 m, molecular sieve 5 column - 10 m, and TCD). Liquid products were collected from experiments performed for 48 h at steady state. Liquid analysis was performed off-line with gas chromatography (Agilent GC 6890 equipped with FID). The mass balance was calculated for each test to ensure the validity of the analysis and only results that were within 5 wt.% mass balance error were accepted. Experiments were repeated at least three times or as many required to meet the mass balance requirement. Error bars were calculated using the standard deviation of the repeated experiments.

2.3. Gas and liquid product analysis

The gas products (H_2, CO, CO_2, C_1-C_4 paraffin, and olefin gasses) were analyzed on-line with gas chromatography. Calibration for all gasses was conducted with gas standards (UHP300 Airgas). The calibration of each paraffin gas was assumed to hold for its corresponding olefin. Gas flowrates out of the reactor were calculated using Ar as internal standard. CO conversion was calculated from the difference of CO flowrates measured at the inlet and the outlet of the reactor using Ar as internal standard, as shown in Eq. (1):

$$X_{CO} = \frac{F_{co}^{in} - F_{CO}^{out}}{F_{CO}^{in}} * 100\%,$$

(1)

where F_{co}^{in} and F_{CO}^{out} are the inlet and outlet volumetric flowrates of CO respectively. Three types of selectivity are reported in this paper: the molar selectivity to each product based on carbon number (C%); the

mass selectivity (wt.%) of gasoline range hydrocarbons (C_5-C_{12}) and C_{13+} in the oil phase; and the mass selectivity (wt.%) of paraffins, isomers and olefins in the oil product. Moreover, the overall gasoline yield was calculated as a fraction of the C_5-C_{12} weight over the total syngas mass fed. C% selectivity was used for peer paper comparison [31–33]. Mass selectivities were used to describe the gasoline selectivity and quality in the oil, as is typical in refinery applications. Gasoline selectivity was calculated to provide a direct and clear metric of the effectiveness of the proposed process in its intended application (production of gasoline). The molar selectivity was calculated with the following equations:

$$S_{c_{1-4}} = \frac{n_{1-4} F_{C_{1-4}}}{F_{CO}^{in} - F_{CO}^{out}} \times 100\%$$

(2)

$$S_{c_{5+}} = (1 - \sum_i \frac{n_i F_{C_i}}{F_{CO}^{in} - F_{CO}^{out}}) \times 100\%$$

(3)

Eq. (2) was used to calculate molar selectivity to CO_2 and C_1-C_4 species. F_{C_i} is the outlet volumetric flowrate of species C_i. n_i is the number of carbon atoms in each species. Eq. (3) was used to calculate C_{5+} selectivity. At the end of each experiment, the liquid products were collected from the wax and cold traps and weighed. Oil and water were separated by decanting with a pipette and were quantified separately. The oil product was dissolved in CS_2, and analyzed with an Agilent GC 7890 equipped with HP-5 column (0.25 μm, 30 m × 0.320 mm, −60–350 °C) and FID. C_5-C_{40} calibration was performed with C_5-C_8 and C_8-C_{40} alkane calibration standards (Sigma-Aldrich). In the liquid GC-FID analysis, oxygenates, alcohols and branched paraffins (here lumped together and termed as isomers) were detected as the peaks before the calibrated alkane peak. α-olefins and other olefins were detected as the peak right before and the peak subsequent to the corresponding alkane peaks, respectively [33].

3. Catalyst characterization

The synthesized monolithic catalysts were ground to a fine powder in an agate mortar for characterization. The Brunauer-Emmett-Teller (BET) surface area of the prepared catalysts was measured with a Micromeritics ASAP 2020 using N_2 physisorption at 77 K. Samples were degassed at 120 °C for 12 h at 10 °C/min. FEI EFEM Quanta 250 SEM and EDAX Genesis EDS were used for Scanning Electron Microscopy (SEM) imaging and Energy Dispersive Spectroscopy (EDS) mapping to determine textural and elemental properties. Prior to characterization, the monolith catalysts were cut with a razor blade and sputter-coated with gold. Line EDS spectrums were taken using 500 ms dwell time and 59 points per line. A Scintag model XDS 1000 was used for X-ray diffraction (XRD) characterization. The scan angle range was set to 5°–80° with 2°/min scan speed. Voltage of 40 kV and current of 44 mA were applied. The Scherrer equation was used to calculate the crystallite size of Co_3O_4 in each catalyst. Transmission electron microscopy (TEM) and Energy Dispersive X-ray Spectroscopy (EDS) were collected using a FEI Talos F200X operating at 200 KV. TEM characterization was performed after completion of the FTS experiments, to assess the properties of the catalysts after reaction.

3.1. Characterization of the fresh structured catalysts

The N_2 sorption isotherms of the catalysts prepared are shown in Fig. 2. The isotherm of pure ZSM-5 is also shown to provide an upper bound for the surface area of the materials prepared. For comparison of the surface area change, the raw monolith and a catalyst with cobalt directly supported on the monolith were also characterized. As shown Fig. 2, adsorption of N_2 increases sharply at P/P0 0–0.1 and 0.9–1 for the ZSM-5, ZSM-5/Co-Al_2O_3/M, and Co-Al_2O_3/M catalysts, confirming a typical type IV isotherm which exhibits micro (0 Å to 20 Å) and macro (> 500 Å) porosity. The physisorption isotherm of the monolith is small
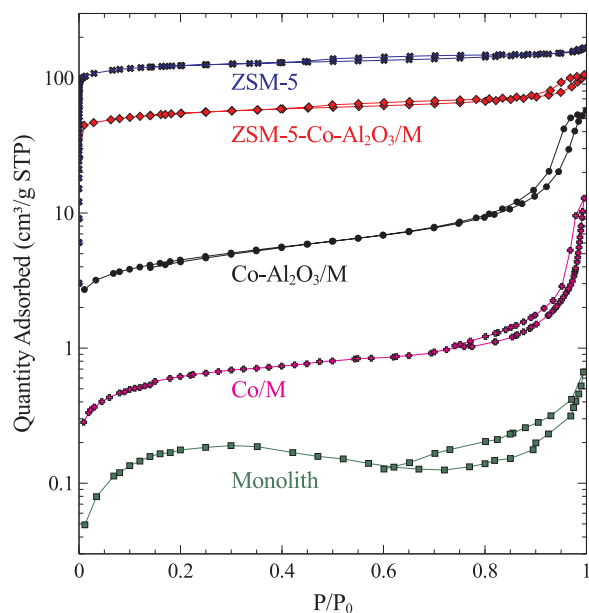
Fig. 2. N_2 adsorption-desorption isotherms of the FTS catalysts and baseline materials.

and flat, indicating a low surface area. The isotherm of the monolith is slightly inaccurate in its shape, probably due to its very small surface area, which is within the error margin of the BET. From Fig. 2, it is clear that coating with Al_2O_3 and ZSM-5 significantly increases the surface area of the monolith support. The shrinking of the adsorption-desorption hysteresis loop from the monolith to the Co/M and Co-Al_2O_3/M materials indicates that the pores of the raw monolith are partially filled with Co and Al_2O_3.

Adsorption data measured for each material is summarized in Table 2. The surface area of the materials studied decreases in the order: ZSM-5 > ZSM-5/Co-Al_2O_3/M > Co-Al_2O_3/M > Co/M > Monolith. By coating the monolith with Al_2O_3, the surface area increased by 25 times, providing a better substrate for active material dispersion and increased catalyst activity, which is also verified later in this work (cf. Table 3). The extensive micro-porosity observed in the ZSM-5 coated material is a clear indication of the membrane formed around the Al_2O_3 layer. This was further confirmed in SEM and EDS analyses, discussed in the following.

Fig. 3 shows the XRD pattern of the fresh structured catalysts (a) ZSM-5/Co-Al_2O_3/M and (b) Co-Al_2O_3/M. XRD peaks were fitted using the D8 EVA software package. The diffraction peaks at 10.45, 18.16, 21.27, 26.37, 28.43, 29.48, 33.93 and 54.3° correspond to the cordierite monolith ($2MgO:2Al_2O_3:5SiO_2$). The peaks at 7.82, 8.76, 13.83,

14.65, 23.06, 23.76, 24.31 and 29.16° are attributed to the ZSM-5 phase. Peaks at 31.27, 36.85, 38.54, 65.24° belong to Co_3O_4 phase. Co signals are very low due to the small loading. ZSM-5 peaks were very clear for the ZSM-5/Co-Al_2O_3/Mc catalysts. The signals associated with the cordierite monolith dropped for the ZSM-5/Co-Al_2O_3/M catalysts compared to Co-Al_2O_3/M which was caused by the introduction of ZSM-5 (about 33 wt%, Table 1). The Co_3O_4 crystallite size was calculated as shown in Table 2.

3.2. Structure of the catalysts

Fig. 4(a) shows the SEM image of the cross-section of a monolith support coated with Al_2O_3, Co_3O_4, and ZSM-5. The corresponding elemental line mapping is shown Fig. 4(b). It is clear in Fig. 4(a) that Al_2O_3 and ZSM-5 form two distinct layers on the monolith with the Al_2O_3 layer directly on the monolith and the ZSM-5 formed on the outer layer. A thicker and round layer forms at the corner of the monolith channel. The elemental mapping in Fig. 4(b) confirms the presence and relative concentration of Al, Si and Co along the red arrow. The Co and Al signals appear and disappear almost at the same scan length. This indicates that Co coexists with the porous Al_2O_3 layer. The Si signal has a sharp increase at 200 μm, while the Co and Al signals have a sharp drop. This indicates that ZSM-5 forms as a distinct outer layer and there is no Co diffusion into the ZSM-5 layer. From Fig. 4(a), the alumina layer thickness was estimated at about 50 μm, while the ZSM-5 layer is about 150 μm thick.

3.3. Transmission electron microscopy and energy dispersive X-ray spectroscopy

TEM images of the Co-Al_2O_3/M and ZSM-5/Co-Al_2O_3/M used catalysts and EDS of the ZSM-5/Co-Al_2O_3/M used catalyst are shown in Fig. 5. The top images show TEM of the Co-Al_2O_3/M and ZSM-5/Co-Al_2O_3/M used catalysts. The bottom images show the EDS of the ZSM-5/Co-Al_2O_3/M used catalyst. The EDS of Co-Al_2O_3/M is not shown here because its surface was contaminated by heavy hydrocarbons. This indicates that the Co-Al_2O_3/M catalyst surface was fouled with heavy hydrocarbons, which were not removed during the reactor purging. The catalysts with ZSM-5 coating did not indicate heavy hydrocarbon fouling in EDS. From Fig. 5(a), the average particle size of dispersed Co (dark spots in Fig. 5(a)) was estimated at ~16 nm, which agrees well with the XRD characterization (Table 2). From Fig. 5(b), the average Co particle size of the ZSM-5/Co-Al_2O_3/M used catalyst was estimated at ~13.3 nm. This indicates that ZSM-5 coating has no effect on catalyst particle size. Co particles are well distributed on both catalysts. The bottom images of Fig. 5 show the EDS of the used ZSM-5/Co-Al_2O_3/M catalyst. Co is supported on the Al_2O_3 layer deposited at the surface of the monolithic substrate, while ZSM-5 (indicated by the rich Si signal) is a separate region without Co deposition.

4. Results and discussion

4.1. ZSM-5 effect on FTS performance and products selectivity

The functionality of the ZSM-5 coating was analyzed in terms of its capacity to enhance cracking and isomerization reactions, as well as its capability to control the size of the hydrocarbons produced. FTS was performed using catalysts with and without ZSM-5 coating to test this hypothesis. Table 3 presents the performance of monolithic catalysts with and without ZSM-5 coating at the same reaction conditions. The data was also used in Fig. 6 to illustrate the corresponding trend.

ZSM-5 coating was responsible for a slight drop in CO conversion in the experiments with ZSM-5/Co-Al_2O_3/M. Since the loading of Co in the Co-Al_2O_3/M catalyst was slightly higher than that in the ZSM-5/Co-Al_2O_3/M (Table 1), it can be concluded that the ZSM-5 coating does not significantly alter the catalyst activity. This is in contrast to previously

Table 2
Structure Parameters of the Materials studied.

Material	S_{BET} (m^2 g^{-1})[a]	V_{total} (cm^3 g^{-1})[b]	V_{micro} (cm^3 g^{-1})[c]	D (nm)[d]	D (nm)[e]
Monolith	0.7	0.0008	0	–	–
Co/M	2.3	0.02	0	–	–
Co-Al_2O_3/M	16.2	0.09	0.0006	14.6	16.0
ZSM-5/Co-Al_2O_3/M	188.3	0.15	0.05	12.8	13.3
ZSM-5	418.8	0.25	0.14	–	–

[a] Surface area obtained from Brunauer-Emmett-Teller (BET) measurements (S_{BET}).
[b] BJH desorption pore volume (V_{total}).
[c] t-plot micro-volume (V_{micro}).
[d] Scherrer's crystallite size (D) of Co_3O_4.
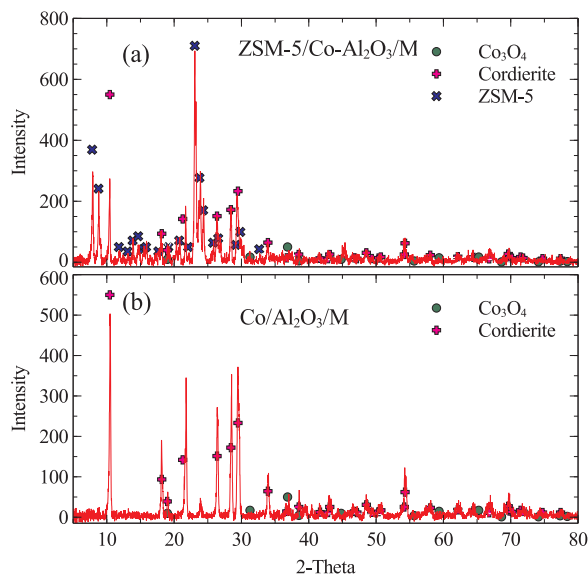[e] Average particle size (D) Calculated from TEM.

Table 3

Performance of Monolith Catalyst with and without ZSM-5. Reaction conditions: Temperature: 230 °C, Pressure: 12 bar, H_2/CO: 2:1, Syngas flowrate: 35 ml/min, Catalyst loading: 2.9 g for ZSM-5/Co-Al_2O_3/M and 2.3 g for Co-Al_2O_3/M, Co loading: 3.3 wt.% for ZSM-5/Co-Al_2O_3/M and 6.5 wt.% for Co-Al_2O_3/M, Time of experiments: 48 h.[a]

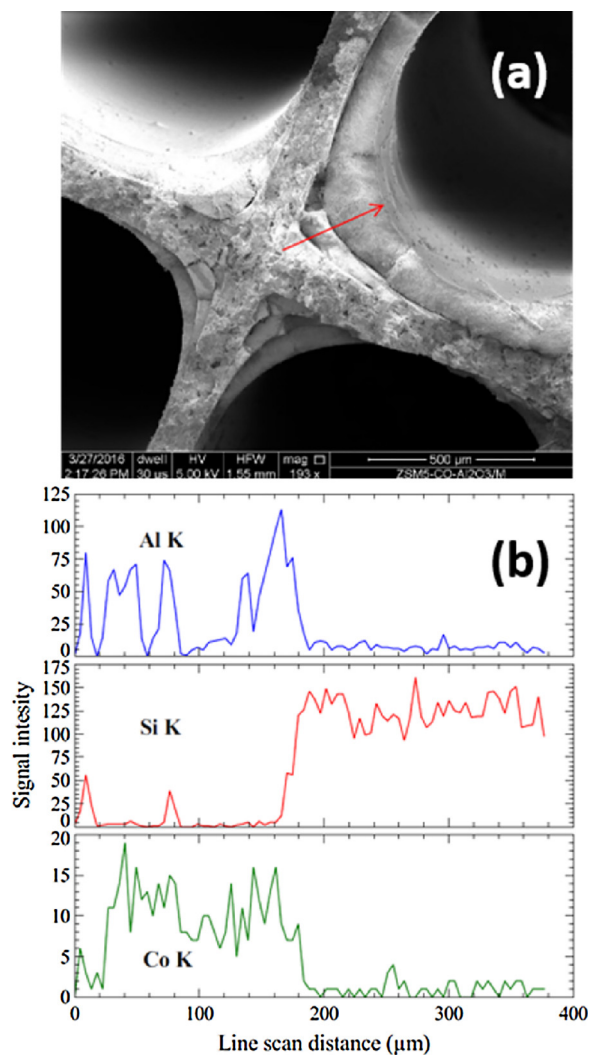| Catalyst	CO conv (%)	Product selectivity (C%)				Oil phase (wt.%)		Oil product selectivity (wt.%)			Mass balance (%)
		CH_4	CO_2	C_2-C_4	C_{5+}	C_5-C_{12}	C_{13+}	Paraffins	Isomers[b]	Olefins	
Co-Al_2O_3/M	81.7 ± 2.6	20.0 ± 0.5	3.8 ± 1.8	16.3 ± 0.7	60.0 ± 3.3	63.3 ± 4.0	35.8 ± 2.8	68.4 ± 5.1	26.3 ± 3.9	4.8 ± 1.3	95.9 ± 0.6
ZSM-5/Co-Al_2O_3/M	78.7 ± 3.7	10.9 ± 1.1	1.5 ± 1.4	12.1 ± 2.8	75.5 ± 0.7	93.3 ± 2.1	6.5 ± 1.8	28.9 ± 1.7	49.8 ± 4.0	21.3 ± 2.3	96.0 ± 0.3

[a] Reference commercial FTS selectivity with Co-based catalysts is reported by de Klerk [34] in wt% {CH4: 5.6, C2-C4: 6.3, C5+: 86.5, (C5-C10)/C5+: 23}, Dry [10] in C% {CH4: 4, C2-C4: 8, C5+: 87, (C5-160 C)/C5+: 22}, and Enger et al. [35] in C% {CH4: 8–11, C5+: 72.4-86.7}.

[b] The lump of isomers includes the oxygenated products (if any).

Fig. 3. XRD patterns of fresh catalysts: (a) Monolith catalyst coated with Al_2O_3, Co_3O_4, and ZSM-5. (b) Monolith catalyst without ZSM-5 coating.

studied synthesis methods of ZSM-5 core-shell catalysts, which showed active site loss from the pretreatment process [36]. It is noteworthy that the CH_4 selectivity decreased to almost half with the use of the ZSM-5 coating. This observation is in agreement with prior work [28,37,38] and has been explained as the result of altered water fugacity due to the hydrophilicity of the zeolite layer [28]; re-adsorption of the zeolite-produced intermediate isomers and olefins and recombination with CH_2 intermediates [28]; balancing of local temperature gradients between exothermic FTS and endothermic zeolite-catalyzed reactions [37]; and the fact that consumption of long-chain FTS products in the zeolite layer may shift FTS selectivity to higher carbon-number products [38]. Sartipi et al. [39] note that hydrogenolysis may increase selectivity to CH_4 in the presence of a zeolite, but they note that literature on this matter is inconsistent. Duyckaerts et al. [40] showed that the presence of CO restores the intrinsic activity of the zeolite for oligomerization of short-chain (α-)olefins, leading to chain-growth and reduction of the overall yield to undesired gas products (C_4-). However, relevant work by Jacobs et al. [35], Rytter et al. [41], and Igelsia [42,43] shows that diffusion limitations (presumably induced by the zeolite layer in this work) change the H_2/CO fugacity ratio on the catalyst surface, leading to excessive chain termination and higher light product selectivities. Overall, the change in H_2/CO local ratios, water fugacity and the impact of isomerization, cracking and hydrogenolysis reactions on the localized temperature gradients needs to be better understood in reactor configurations that, unlike the one presented here, focus on local phenomena, instead of reactor-level results. A possible explanation for the lower selectivity to C_2-C_4 hydrocarbons is provided by

Fig. 4. (a) Monolith catalyst coated with Al_2O_3, Co_3O_4, and ZSM-5. (b) Al, Si and Co line mapping along the red arrow from (a) (For interpretation of the references to colour in this figure legend, the reader is referred to the web version of this article).

Halmenschlager et al. [44] and Ismagilov et al. [45] who conducted research on ZSM-5 oligomerization with FTS tail gas. Their analysis showed that ZSM-5 can oligomerize light hydrocarbons, especially ethylene and butylene into liquid hydrocarbons, such as, dimers and trimers, thus decreasing light hydrocarbons selectivity. Most importantly, Fig. 6 shows that the mass selectivity to C_5-C_{12} (Gasoline range) range product increased significantly with the ZSM-5/Co-Al_2O_3/M catalyst. The C_5-C_{12} liquid product selectivity reached 93.3 wt.%
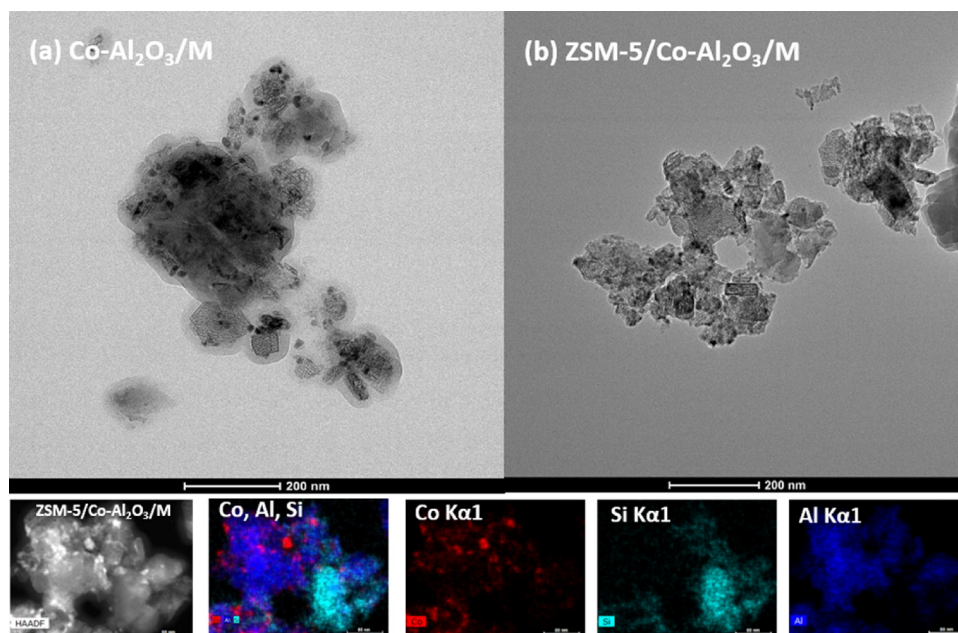
Fig. 5. Top: TEM image for (a) $Co-Al_2O_3/M$ used catalyst, (b) $ZSM-5/Co-Al_2O_3/M$ used catalyst. Bottom: EDS for $ZSM-5/Co-Al_2O_3/M$ used catalyst.

(Table 3), which is comparable with the results of Sun et al. [46] and Bao et al. [28]. In Fig. 6, the gasoline yields for catalysts with and without ZSM-5 coating are shown (last plot in Fig. 6). Gasoline yield for catalysts coated with ZSM-5 reached 20 wt.% which is double that of catalysts without ZSM-5 coating. The reason for the yield improvement is the cracking, isomerization, and oligomerization reactions over the ZSM-5 catalyst membrane. Hydrocracking and isomerization reactions shifted the selectivity of heavy hydrocarbons ($> C_{12}$) to lighter products (C_5-C_{12}), while oligomerization reactions decreased the C_2-C_4 selectivity and favored products in the desired C_5-C_{12} range [30,47]. It can be concluded that the combination of a structured support with a ZSM-5 membrane resulted in a highly active and gasoline selective FTS catalyst.

The liquid product distribution as a function of carbon number is shown in Fig. 7. The $Co-Al_2O_3/M$ catalyst was selective to heavy hydrocarbons up to C_{28}, which is in good agreement with earlier reports [30,40,48–50]. As shown in Fig. 7(a), ZSM-5 coating led to a shift of

selectivity from heavy hydrocarbons ($> C_{15}$) to light hydrocarbons. The selectivity peak for the $ZSM-5/Co-Al_2O_3/M$ catalyst was at C_8, which indicates a high-octane and a high-quality gasoline product. The same conclusion can be drawn from Fig. 7(b) and (c). The selectivity to isomers reached 49.8 wt.% (Table 3), which is about 15 wt.% higher than previously reported values for FTS [24]. Hydrocracking and isomerization over the ZSM-5 coated catalysts were very extensive, as shown by the increased isomer and olefin content. In summary, monolith catalysts coated with ZSM-5 membrane showed high activity and high selectivity towards gasoline range products under normal FTS conditions.

4.2. Temperature effect on ZSM-5 coated monolith catalysts performance

The performance of the $ZSM-5/Co-Al_2O_3/M$ catalyst at different temperatures is summarized in Table 4 and plotted in Fig. 8. CO conversion increased significantly with temperature in the 210–230 °C
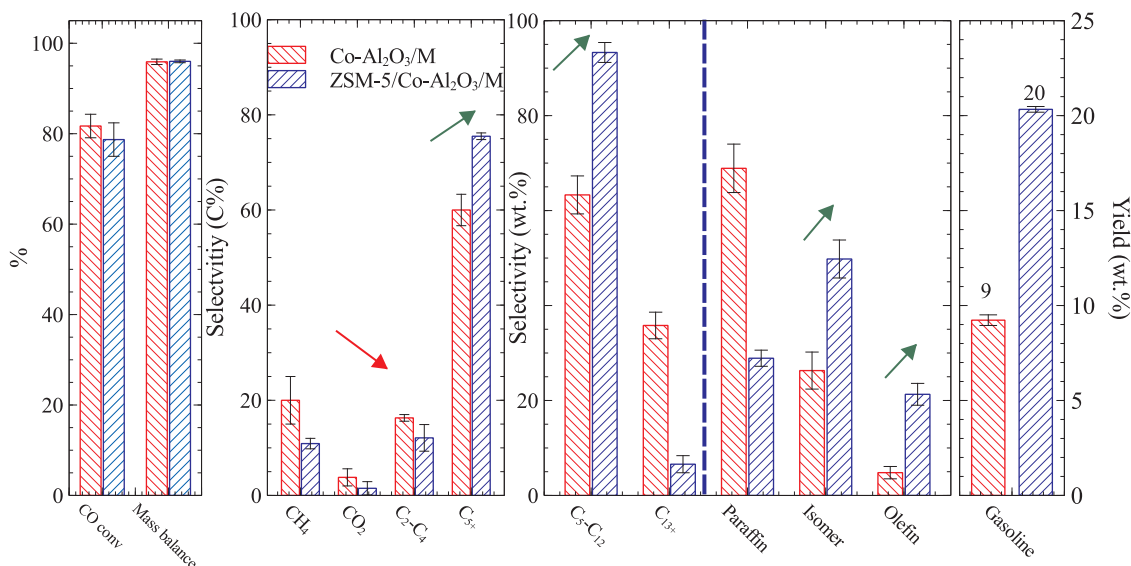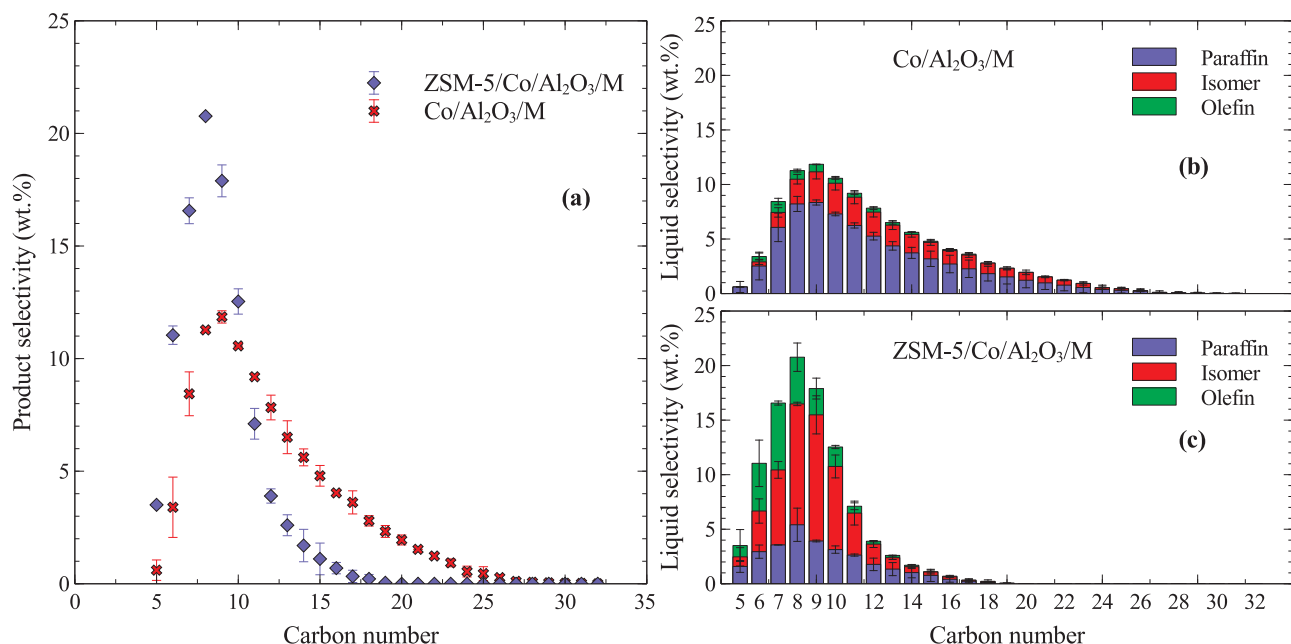

Fig. 6. Overall performance summary for catalyst with and without ZSM-5 coating. Reaction conditions as noted in Table 3.

Fig. 7. The liquid hydrocarbon distribution. (a) Selectivity of different carbon number species for Co-Al$_2$O$_3$/M and ZSM-5/Co-Al$_2$O$_3$-M. (b) (c) Paraffin, isomer, olefin selectivity as a function of carbon number for Co-Al$_2$O$_3$/M and ZSM-5/Co-Al$_2$O$_3$/M. Reaction conditions as noted in Table 3.

range. Further increasing the temperature did not affect CO conversion, indicating that a kinetic limit between competing reactions had been reached. CH$_4$ selectivity was lowest at the intermediate temperature of 230 °C. CO$_2$ selectivity increased slightly with the temperature increase, which could be attributed to the water-gas shift reaction at higher temperatures over the Co catalysts [21,48]. Selectivity to C$_2$-C$_4$ did not change significantly with the change in temperature in the range studied. The ZSM-5/Co-Al$_2$O$_3$/M catalyst showed better cracking and isomerization activity at elevated temperatures. This can be seen from the substantial increase in the selectivity to isomers and the corresponding decrease in C$_{13+}$ selectivity. Industrial hydrocrackers operate in the temperature range of 350–440 °C [51], and the temperatures studied here were selected as a compromise between optimal FTS and refinery operations. The selectivity to C$_{5+}$ reached a maximum at 230 °C (Fig. 8), while it decreased when temperature increased to 250 °C. This is anticipated for the effect of temperature on FTS, where elevated temperatures lead to higher CH$_4$ and C$_2$-C$_4$ selectivity [21]. At the low temperature studied cracking and isomerization were limited. At high temperature, unfavored short chain hydrocarbons were formed. Within the three temperatures tested, gasoline yield reached highest at 230 °C.

The liquid product selectivity as a function of temperature is shown in Fig. 9. The liquid hydrocarbons from experiments at 230 °C and 250 °C were distributed within gasoline range carbon numbers. The liquid product from the 210 °C experiments follows the ASF distribution with up to C$_{23}$ products identified. This is in agreement with the known Co-catalyzed FTS optimal temperature. Increasing the temperature enhanced the activity of the ZSM-5 layer in cracking lengthy hydrocarbon

chains, while isomer and olefin selectivity also improved. At the higher temperature, higher carbon number products isomerized more extensively. Liquid products that do not precisely follow the ASF distribution were formed at 230 °C and 250 °C.

In summary, ZSM-5 coated catalysts produced more isomers and olefins in the liquid product, improving its quality at higher temperature. However, the high temperature also promoted FTS side reactions and favored undesired gas products. A moderate temperature should be chosen for maximum gasoline production. In this work, it was 230 °C.

4.3. Pressure effect on ZSM-5 coated monolith catalyst performance

The effect of pressure on FTS over the ZSM-5 coated monolith catalysts is summarized in Table 5 and Fig. 10. CO conversion decreased with increasing pressure, which indicated limitations of mass and heat transfer introduced by the ZSM-5 layer and the liquid products layer formed during the reaction. The selectivity to CH$_4$, CO$_2$ and C$_2$-C$_4$ hydrocarbons showed a monotonic decline with increasing pressure (Fig. 10). This is common and reasonable for the effect of pressure on FTS [22,51]. C$_{5+}$ molar selectivity reached the highest at 20 bar, while gasoline selectivity was highest at 12 bar. With the ZSM-5 catalyzed cracking becoming less favorable at higher pressures, longer hydrocarbon chains formed at 20 bar. Although the total C$_{5+}$ selectivity increased with pressure, the gasoline yield exhibited a peak at 12 bar. At 6 bar, fewer long-chain hydrocarbons were formed (leading to fewer gasoline-range products from ZSM-5 cracking); while at 20 bar, too many long-chain hydrocarbons were produced resulting in plugging and deteriorating the ZSM-5. Paraffin selectivity increased with

Table 4

Conversion and Selectivity Summary of ZSM-5/Co-Al$_2$O$_3$/M Catalyst as a Function of Temperature. Reaction conditions: Catalyst loading: 2.9 g, Co loading: 3.3 wt.%, Pressure: 12 bar, H$_2$/CO ratio: 2:1, Syngas flowrate: 35 ml/min, Time on stream: 48 h. Reference commercial selectivities are reported in Table 3.

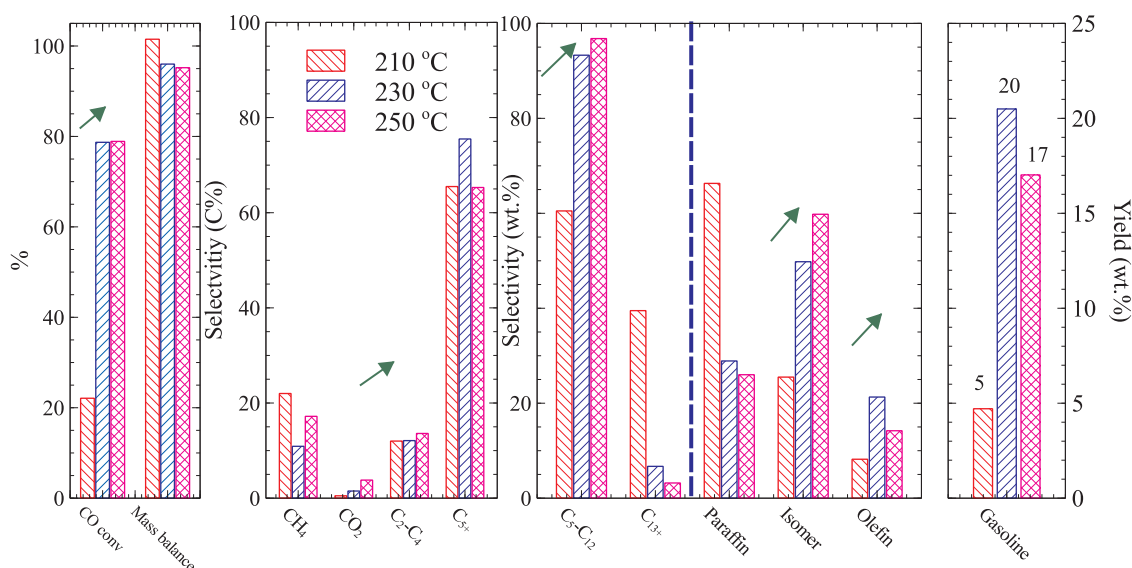| T (°C)	CO Conv. (%)	Product selectivity (C%)				Oil phase selectivity (wt.%)		Oil product selectivity (wt.%)			Mass Balance (%)
		CH$_4$	CO$_2$	C$_2$-C$_4$	C$_{5+}$	C$_5$-C$_{12}$	C$_{13+}$	Paraffins	Isomers	Olefins	
210	22.1	22.0	0.5	12.0	65.5	60.5	39.5	66.3	25.5	8.2	101.5
230	78.7	10.9	1.5	12.1	75.5	93.3	6.7	28.9	49.8	21.3	96.0
250	78.9	17.2	3.8	13.6	65.3	96.8	3.2	26	59.8	14.2	95.2

Fig. 8. Overall performance summary of temperature effect for catalyst with ZSM-5 coating. Reaction conditions as noted in Table 4.
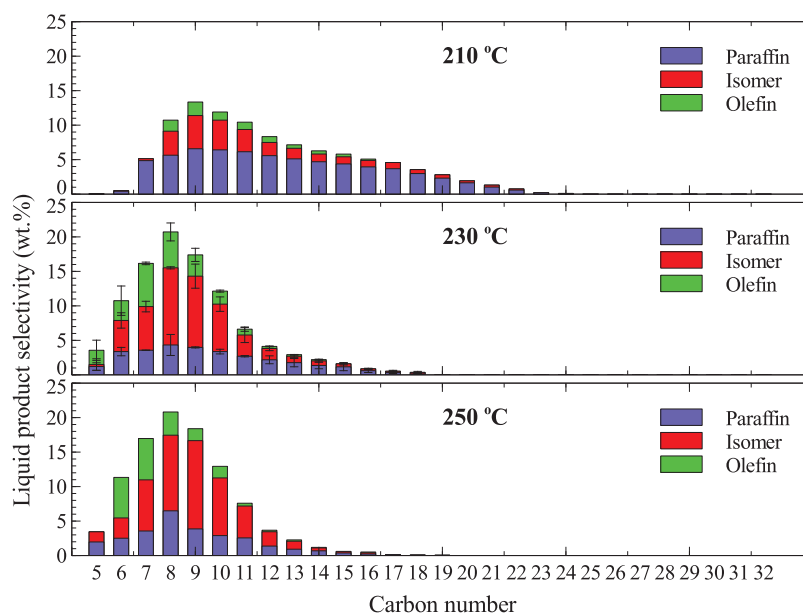

Fig. 9. Liquid hydrocarbons selectivity from FTS at different temperatures. Reaction conditions as noted in Table 4.

Table 5

FTS Performance Summary of ZSM-5/Co-Al$_2$O$_3$/M Catalyst at Different Pressures. Reaction conditions: Catalyst loading: 2.9 g, Co loading: 3.3 wt.%, T: 230 °C, H$_2$/CO ratio: 2:1, syngas flowrate: 35 ml/min, Time on stream: 48 h. Reference commercial selectivities are reported in Table 3.

P (bar)	CO Conv. (%)	Product selectivity (C%)				Oil phase selectivity (wt.%)		Oil products selectivity (wt.%)			Mass Balance (%)
		CH$_4$	CO$_2$	C$_2$-C$_4$	C$_{5+}$	C$_5$-C$_{12}$	C$_{13+}$	Paraffins	Isomers	Olefins	
6	81.6	17.3	4.0	14.6	64.1	96.3	3.7	24.7	50	25.3	94.8
12	78.7	10.9	1.5	12.1	75.5	93.3	6.8	28.9	49.8	21.3	96.0
20	63.2	10.2	0.7	9.2	79.9	79.3	20.7	40.3	39.8	19.9	96.9

pressure, while isomers and olefins decreased. This is due to more severe reabsorption and decreased chain branching reactions. Chain branching has been reported to become less favorable at high pressure, while this trend is opposite for reabsorption [21,52]. Reabsorption of olefins can result in longer paraffin chains. Within the tested pressures, 12 bar showed the highest gasoline yield.

The distribution of liquid hydrocarbons is plotted in Fig. 11. Higher pressure was shown to favor the formation of longer chain

hydrocarbons. Hydrocarbon chains reached C$_{21+}$ at 20 bar, while the vast majority was smaller than C$_{12}$ at 6 bar. Selectivity to isomers and olefins decreased with pressure. This is in agreement with Sarkari et al. [53] who reported that olefin reactivity increased because of the condensation of the hydrocarbons at high pressure. Since the ZSM-5 cracking and isomerization are significant but not dominant at 230 °C, the pressure had a relatively more pronounced effect on the liquid product distribution. Low pressure favored the production of smaller
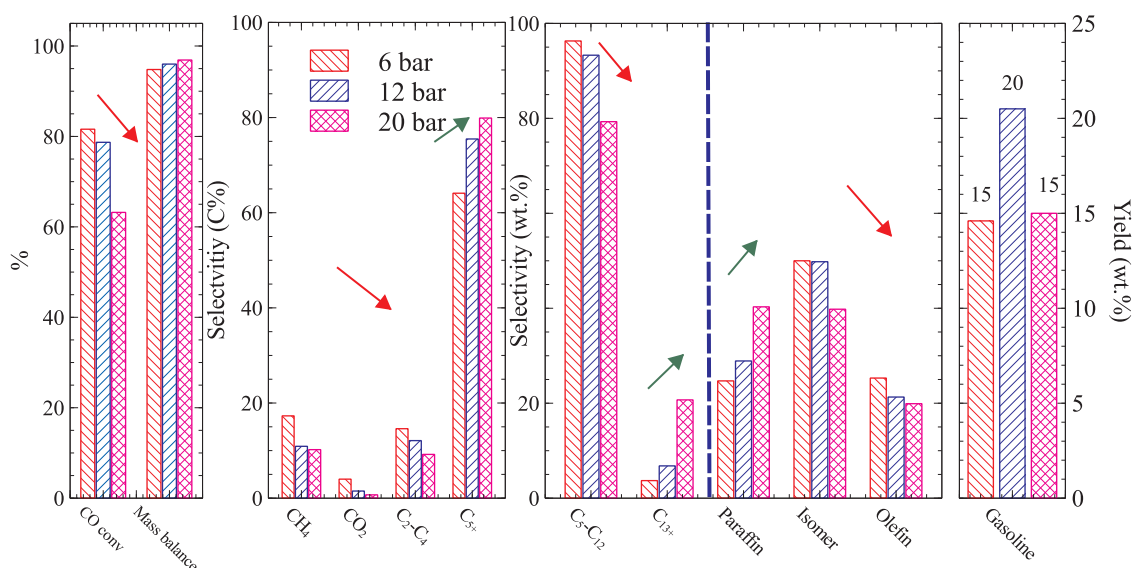
Fig. 10. Overall performance summary of pressure effect for catalyst with ZSM-5 coating. Reaction conditions as noted in Table 5.
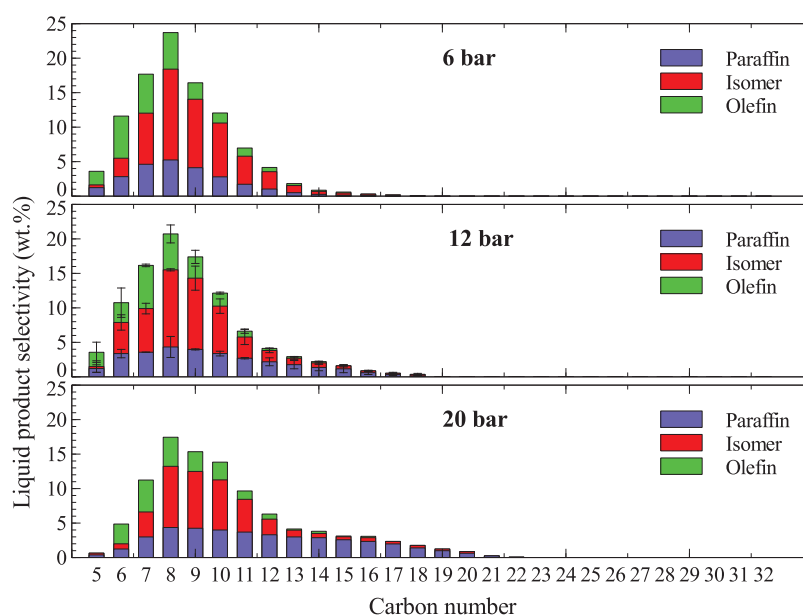

Fig. 11. Liquid hydrocarbon selectivity from FTS at different pressures. Reaction conditions as noted in Table 5.

hydrocarbons, in the gasoline range. It also favored the production of undesired gas, in lieu of gasoline yield. In this work, pressure of 12 bar was found to be best for high yields to high octane rating gasoline. Overall, the structured catalysts show a peak in conversion and selectivity at 230 °C, a temperature slightly higher than what is commercially exercised (220 °C for Co catalysts), but at significantly lower pressure (12 bar compared to 20–30 bar in commercial applications). This reduction in pressure requirements, may be beneficial from the process economics and environmental perspectives, as lower pressures should decrease the operating cost and energy requirements of the FTS process.

4.4. Conclusions

A novel structured catalyst for in-situ FTS product upgrading to gasoline-range hydrocarbons was synthesized. This catalyst was tested to explore the hypothesis that combination of the intensified process efficiency of monolith with the isomerization and cracking capacity of

ZSM-5 can enhance FTS selectivity to gasoline range products. Monolith-supported Co catalysts coated with ZSM-5 showed high FTS selectivity to gasoline range products (C_5-C_{12}) at 230 °C and 12 bar. Gasoline selectivity was found to be as high as 93.3 wt.% within the 75.5% C_{5+} oil product and CO conversion was as high as 78.7%. The addition of ZSM-5 on the monolith catalyst not only improved the gasoline selectivity but also gasoline quality, in terms of olefin and isomer composition. Investigation of the temperature effect on catalyst performance showed that the liquid product selectivity shifted to hydrocarbons of lower carbon numbers with the increase of temperature. CO_2 selectivity increased sharply with temperature, because of the enhancement of the water gas shift reaction. More isomers and olefins were produced over the ZSM-5-coated monoliths at high temperatures, but at the expense of the liquid product yield. Increasing reaction pressure led to higher selectivity to heavy hydrocarbons. Low pressure favored the production of isomers and olefins. High pressure was shown to introduce diffusion limitations to the ZSM-5 layer of the FTS catalysts synthesized. A moderate pressure of 12 bar was proposed to favor

gasoline production.

Acknowledgements

This work was financially supported by the American Chemical Society – Petroleum Research Fund, grant No: 53648-DNI5.

References

[1] A.T. Bell, B.C. Gates, D. Ray, M.R. Thompson, Basic Research Needs: Catalysis for Energy, DOE SC Basic Energy Sciences, Richland, WA, 2008, http://dx.doi.org/10.2172/927492.

[2] S. Du, D.P. Gamliel, M.V. Giotto, J.A. Valla, G.M. Bollas, Coke formation of model compounds relevant to pyrolysis bio-oil over ZSM-5, Appl. Catal. A Gen. 513 (2016) 67–81, http://dx.doi.org/10.1016/j.apcata.2015.12.022.

[3] S. Du, J.A. Valla, R.S. Parnas, G.M. Bollas, Conversion of polyethylene terephthalate based waste carpet to Benzene-Rich oils through thermal, catalytic, and catalytic steam pyrolysis, ACS Sustain. Chem. Eng. 4 (2016) 2852–2860, http://dx.doi.org/10.1021/acssuschemeng.6b00450.

[4] R.K. Dixon, E. McGowan, G. Onysko, R.M. Scheer, US energy conservation and efficiency policies: challenges and opportunities, Energy Policy 38 (2010) 6398–6408, http://dx.doi.org/10.1016/j.enpol.2010.01.038.

[5] G. Bang, Energy security and climate change concerns: triggers for energy policy change in the United States? Energy Policy 38 (2010) 1645–1653, http://dx.doi.org/10.1016/j.enpol.2009.01.045.

[6] R.M. de Deugd, R.B. Chougule, M.T. Kreutzer, F.M. Meeuse, J. Grievink, F. Kapteijn, J.A. Moulijn, Is a monolithic loop reactor a viable option for Fischer–Tropsch synthesis? Chem. Eng. Sci. 58 (2003) 583–591, http://dx.doi.org/10.1016/S0009-2509(02)00583-3.

[7] R.M. de Deugd, F. Kapteijn, J.A. Moulijn, Trends in Fischer–Tropsch reactor technology—opportunities for structured reactors, Top. Catal. 26 (2003) 29–39, http://dx.doi.org/10.1023/B:TOCA.0000012985.60691.67.

[8] R.M. de Deugd, F. Kapteijn, J.A. Moulijn, Using monolithic catalysts for highly selective Fischer–Tropsch synthesis, Catal. Today 79–80 (2003) 495–501, http://dx.doi.org/10.1016/S0920-5861(03)00073-7.

[9] A.Y. Khodakov, W. Chu, P. Fongarland, Advances in the Development of Novel Cobalt Fischer − Tropsch Catalysts for Synthesis of Long-Chain Hydrocarbons and Clean Fuels, Chem. Rev 107 (2007) 1692–1744, http://dx.doi.org/10.1021/cr050972v.

[10] M.E. Dry, High quality diesel via the Fischer-Tropsch process - a review, J. Chem. Technol. Biotechnol. 77 (2002) 43–50, http://dx.doi.org/10.1002/jctb.527.

[11] R.P. Marin, S.A. Kondrat, J.R. Gallagher, D.I. Enache, P. Smith, P. Boldrin, T.E. Davies, J.K. Bartley, G.B. Combes, P.B. Williams, S.H. Taylor, J.B. Claridge, M.J. Rosseinsky, G.J. Hutchings, Preparation of Fischer–Tropsch supported cobalt catalysts using a new gas anti-solvent process, ACS Catal. 3 (2013) 764–772, http://dx.doi.org/10.1021/cs4000359.

[12] K. Pangarkar, T.J. Schildhauer, J.R. van Ommen, J. Nijenhuis, J.A. Moulijn, F. Kapteijn, Experimental and numerical comparison of structured packings with a randomly packed bed reactor for Fischer-Tropsch synthesis, Catal. Today 147 (2009) 2–9, http://dx.doi.org/10.1016/j.cattod.2009.07.035.

[13] N.E. Tsakoumis, M. Rønning, Ø. Borg, E. Rytter, A. Holmen, Deactivation of cobalt based Fischer–Tropsch catalysts: a review, Catal. Today 154 (2010) 162–182, http://dx.doi.org/10.1016/j.cattod.2010.02.077.

[14] B.H. Davis, Fischer–Tropsch synthesis: overview of reactor development and future potentialities, Top. Catal. 32 (2005) 143–168, http://dx.doi.org/10.1007/s11244-005-2886-5.

[15] F. Kapteijn, R.M. de Deugd, J.A. Moulijn, Fischer–Tropsch synthesis using monolithic catalysts, Catal. Today 105 (2005) 350–356, http://dx.doi.org/10.1016/j.cattod.2005.06.063.

[16] F.G. Botes, W. Böhringer, The addition of HZSM-5 to the Fischer − Tropsch process for improved gasoline production, Appl. Catal. A Gen. 267 (2004) 217–225, http://dx.doi.org/10.1016/j.apcata.2004.03.006.

[17] R. Guettel, J. Knochen, U. Kunz, M. Kassing, T. Turek, Preparation and catalytic evaluation of cobalt-based monolithic and powder catalysts for Fischer - Tropsch synthesis, Ind. Eng. Chem. Res. (2008) 6589–6597.

[18] T.A. Nijhuis, A.E.W. Beers, T. Vergunst, I. Hoek, F. Kapteijn, J. Moulijn, Preparation of monolithic catalysts, Catal. Rev. 43 (2001) 345–380, http://dx.doi.org/10.1081/CR-120001807.

[19] Q. Zhang, J. Kang, Y. Wang, Development of novel catalysts for Fischer-Tropsch synthesis: tuning the product selectivity, ChemCatChem. 2 (2010) 1030–1058, http://dx.doi.org/10.1002/cctc.201000071.

[20] G.P. van der Laan, A.A.C.M. Beenackers, Intrinsic kinetics of the gas–solid Fischer–Tropsch and water gas shift reactions over a precipitated iron catalyst, Appl. Catal. A Gen. 193 (2000) 39–53, http://dx.doi.org/10.1016/S0926-860X(99)00412-3.

[21] G.P. van der Laan, A.A.C.M. Beenackers, Kinetics and selectivity of the Fischer–Tropsch synthesis: a literature review, Catal. Rev. 41 (1999) 255–318, http://dx.doi.org/10.1081/CR-100101170.

[22] M.E. Dry, J.R. Anderson, M. Boudart (Eds.), The Fischer-Tropsch Synthesis, vol. I, Springer US, New York, 1981Catal. Sci. Technol.

[23] M.E. Dry, Practical and theoretical aspects of the catalytic Fischer-Tropsch process, Appl. Catal. A Gen. 138 (1996) 319–344, http://dx.doi.org/10.1016/0926-860X(95)00306-1.

[24] C. Xing, W. Shen, G. Yang, R. Yang, P. Lu, J. Sun, Y. Yoneyama, N. Tsubaki, Completed encapsulation of cobalt particles in mesoporous H-ZSM-5 zeolite catalyst for direct synthesis of middle isoparaffin from syngas, Catal. Commun. 55 (2014) 53–56, http://dx.doi.org/10.1016/j.catcom.2014.06.018.

[25] G. Yang, D. Wang, Y. Yoneyama, Y. Tan, N. Tsubaki, Facile synthesis of H-type zeolite shell on a silica substrate for tandem catalysis, Chem. Commun. 48 (2012) 1263, http://dx.doi.org/10.1039/c2cc16713a.

[26] N. Tsubaki, Y. Yoneyama, K. Michiki, K. Fujimoto, Three-component hybrid catalyst for direct synthesis of isoparaffin via modified Fischer-Tropsch synthesis, Catal. Commun. 4 (2003) 108–111, http://dx.doi.org/10.1016/S1566-7367(03)00003-7.

[27] J.J. He, B.L. Xu, Y. Yoneyama, N. Nishiyama, N. Tsubaki, Designing a new kind of capsule catalyst and its application for direct synthesis of middle isoparaffins from synthesis gas, Chem. Lett. 34 (2005) 148–149, http://dx.doi.org/10.1246/Cl.2005.148.

[28] J. Bao, J. He, Y. Zhang, Y. Yoneyama, N. Tsubaki, A Core/Shell catalyst produces a spatially confined effect and shape selectivity in a consecutive reaction, Angew. Chemie Int. Ed. 47 (2008) 353–356, http://dx.doi.org/10.1002/anie.200703335.

[29] C. Li, H. Xu, Y. Kido, Y. Yoneyama, Y. Suehiro, N. Tsubaki, A capsule catalyst with a zeolite membrane prepared by direct liquid membrane crystallization, ChemSusChem 5 (2012) 862–866, http://dx.doi.org/10.1002/cssc.201100431.

[30] C. Xing, J. Sun, Q. Chen, G. Yang, N. Muranaka, P. Lu, W. Shen, P. Zhu, Q. Wei, J. Li, J. Mao, R. Yang, N. Tsubaki, Tunable isoparaffin and olefin yields in Fischer-Tropsch synthesis achieved by a novel iron-based micro-capsule catalyst, Catal. Today 251 (2015) 41–46, http://dx.doi.org/10.1016/j.cattod.2014.10.022.

[31] T. Fu, Z. Li, Highly dispersed cobalt on N-doped carbon nanotubes with improved Fischer–Tropsch synthesis activity, Catal. Commun. 47 (2014) 54–57, http://dx.doi.org/10.1016/j.catcom.2014.01.008.

[32] L. Zhong, F. Yu, Y. An, Y. Zhao, Y. Sun, Z. Li, T. Lin, Y. Lin, X. Qi, Y. Dai, L. Gu, J. Hu, S. Jin, Q. Shen, H. Wang, Cobalt carbide nanoprisms for direct production of lower olefins from syngas, Nature 538 (2016) 84–87, http://dx.doi.org/10.1038/nature19786.

[33] A. Kasht, R. Hussain, M. Ghouri, J. Blank, N.O. Elbashir, Product analysis of supercritical Fischer-Tropsch synthesis: utilizing a unique on-line and off-line gas chromatographs setup in a bench-scale reactor unit, Am. J. Anal. Chem. 06 (2015) 659–676, http://dx.doi.org/10.4236/ajac.2015.68064.

[34] A. de Klerk, Fischer–Tropsch fuels refinery design, Energy Environ. Sci. 4 (2011) 1177, http://dx.doi.org/10.1039/c0ee00692k.

[35] B.C. Enger, Å.L. Fossan, Ø. Borg, E. Rytter, A. Holmen, Modified alumina as catalyst support for cobalt in the Fischer-Tropsch synthesis, J. Catal. 284 (2011) 9–22, http://dx.doi.org/10.1016/j.jcat.2011.08.008.

[36] X. Li, J. He, M. Meng, Y. Yoneyama, N. Tsubaki, One-step synthesis of H–β zeolite-enwrapped Co/Al2O3 Fischer–Tropsch catalyst with high spatial selectivity, J. Catal. 265 (2009) 26–34, http://dx.doi.org/10.1016/j.jcat.2009.04.009.

[37] G. Yang, C. Xing, W. Hirohama, Y. Jin, C. Zeng, Y. Suehiro, T. Wang, Y. Yoneyama, N. Tsubaki, Tandem catalytic synthesis of light isoparaffin from syngas via Fischer-Tropsch synthesis by newly developed core-shell-like zeolite capsule catalysts, Catal. Today 215 (2013) 29–35, http://dx.doi.org/10.1016/j.cattod.2013.01.010.

[38] J.-Y. Liu, J.-F. Chen, Y. Zhang, Cobalt-imbedded zeolite catalyst for direct syntheses of gasoline via Fischer–Tropsch synthesis, Catal. Sci. Technol. 3 (2013) 2559, http://dx.doi.org/10.1039/c3cy00458a.

[39] S. Sartipi, M. Makkee, F. Kapteijn, J. Gascon, Catalysis engineering of bifunctional solids for the one-step synthesis of liquid fuels from syngas: a review, Catal. Sci. Technol. 4 (2014) 893–907, http://dx.doi.org/10.1039/C3CY01021J.

[40] N. Duyckaerts, I.-T. Trotuş, A.-C. Swertz, F. Schüth, G. Prieto, In situ hydrocracking of Fischer–Tropsch hydrocarbons: co-prompted diverging reaction pathways for paraffin and α-Olefin primary products, ACS Catal. 6 (2016) 4229–4238, http://dx.doi.org/10.1021/acscatal.6b00904.

[41] E. Rytter, N.E. Tsakoumis, A. Holmen, On the selectivity to higher hydrocarbons in co-based Fischer-Tropsch synthesis, Catal. Today 261 (2016) 3–16, http://dx.doi.org/10.1016/j.cattod.2015.09.020.

[42] E. Iglesia, Fischer-tropsch synthesis on cobalt catalysts: structural requirements and reaction pathways, Stud. Surf. Catal. 107 (1997) 153–162, http://dx.doi.org/10.1016/S0167-2991(97)80328-X.

[43] E. Iglesia, S.L.L. Soled, J.E.E. Baumgartner, S.C.C. Reyes, Synthesis and catalytic properties of eggshell cobalt catalysts for the Fischer-Tropsch synthesis, J. Catal. 153 (1995) 108–122, http://dx.doi.org/10.1006/jcat.1995.1113.

[44] C.M. Halmenschlager, M. Brar, I.T. Apan, A. de Klerk, Oligomerization of Fischer–Tropsch tail gas over H-ZSM-5, Ind. Eng. Chem. Res. 55 (2016) 13020–13031, http://dx.doi.org/10.1021/acs.iecr.6b03861.

[45] Z.R. Ismagilov, E.V. Matus, L.T. Tsikoza, Direct conversion of methane on Mo/ZSM-5 catalysts to produce benzene and hydrogen: achievements and perspectives, Energy Environ. Sci. 1 (2008) 526, http://dx.doi.org/10.1039/b810981h.

[46] B. Sun, G. Yu, J. Lin, K. Xu, Y. Pei, S. Yan, M. Qiao, K. Fan, X. Zhang, B. Zong, A highly selective Raney Fe@HZSM-5 Fischer–Tropsch synthesis catalyst for gasoline production: one-pot synthesis and unexpected effect of zeolites, Catal. Sci. Technol. 2 (2012) 1625, http://dx.doi.org/10.1039/c2cy20155k.

[47] M. Yao, N. Yao, Y. Shao, Q. Han, C. Ma, C. Yuan, C. Li, X. Li, New insight into the activity of ZSM-5 supported Co and CoRu bifunctional Fischer-Tropsch synthesis catalyst, Chem. Eng. J. 239 (2014) 408–415, http://dx.doi.org/10.1016/j.cej.2013.11.050.

[48] S. Sartipi, M. Alberts, M.J. Meijerink, T.C. Keller, J. Pérez-Ramírez, J. Gascon, F. Kapteijn, Towards liquid fuels from biosyngas: effect of zeolite structure in Hierarchical-zeolite-Supported cobalt catalysts, ChemSusChem 6 (2013) 1646–1650, http://dx.doi.org/10.1002/cssc.201300339.

[49] S. Sartipi, J.E. van Dijk, J. Gascon, F. Kapteijn, Toward bifunctional catalysts for the direct conversion of syngas to gasoline range hydrocarbons: H-ZSM-5 coated Co

versus H-ZSM-5 supported Co, Appl. Catal. A Gen. 456 (2013) 11–22, http://dx.doi.org/10.1016/j.apcata.2013.02.012.

[50] J. He, Z. Liu, Y. Yoneyama, N. Nishiyama, N. Tsubaki, Multiple-functional capsule catalysts: a tailor-made confined reaction environment for the direct synthesis of middle isoparaffins from syngas, Chem. A Eur. J. 12 (2006) 8296–8304, http://dx.doi.org/10.1002/chem.200501295.

[51] S. Brown, Catalysis in the refining of Fischer-Tropsch syncrude, Platin. Met. Rev. 55 (2011) 263–267, http://dx.doi.org/10.1595/147106711X593717.

[52] G.R. Johnson, S. Werner, A.T. Bell, An investigation into the effects of Mn promotion on the activity and selectivity of Co/SiO 2 for Fischer–Tropsch synthesis: evidence for enhanced CO adsorption and dissociation, ACS Catal. 5 (2015) 5888–5903, http://dx.doi.org/10.1021/acscatal.5b01578.

[53] M. Sarkari, F. Fazlollahi, A. Razmjooie, A.A. Mirzaei, Fisher-Tropsch synthesis on alumina supported iron-nickel catalysts: effect of preparation methods, Chem. Biochem. Eng. Q. 25 (2011) 289–297.